Supporting Information containing 26 pages, 1 table and 10 figures to accompany manuscript titled

Iron redox transformations in the presence of natural organic matter: effect of calcium

Chao Jiang, Shikha Garg and T. David Waite*

School of Civil and Environmental Engineering, The University of New South Wales

Sydney, NSW 2052, Australia

Environmental Science and Technology

August 2017

*Corresponding author: Tel. +61-2-9385 5060; Email d.waite@unsw.edu.au

S1: Background

Based on the findings of our earlier work,[1-3] the Fe redox transformations in non-irradiated SRFA solution is due to the presence of hydroquinone-like moieties (represented by A^{2-}) in SRFA which, on reaction with Fe(III), form Fe(II) and semiquinone-like moieties (A^{-}). The so formed semiquinone-like moieties may in turn oxidize Fe(II) to Fe(III) as indicated in the reaction:

$$A^{2-} + \text{Fe(III)} \underset{k_2}{\overset{k_1}{\rightleftharpoons}} A^{-} + \text{Fe(II)} \qquad (1)$$

with both A^{2-} and A^{-} being long-lived (> 24h) in the dark. [3]

Our earlier work[3] showed that Fe(II) oxidation by dioxygen is very slow under acidic conditions as was confirmed by the very small (10-15% in 1 hour at pH 4) decrease in the Fe(II) concentration when Fe(II) is added to non-irradiated SRFA solution. This observation further supports the contention that no organic moiety capable of oxidizing Fe(II) is intrinsically present in SRFA. Although Fe(II) oxidation by A^{-} was unimportant when Fe(II) was added to non-irradiated SRFA solution (since no A^{-} exist in these solution), it plays an important role in controlling the concentration of Fe(II) generated on Fe(III) reduction in non-irradiated SRFA solution. As shown in eq. 1, any A^{-} generated as a result of oxidation of A^{2-} by Fe(III), oxidizes Fe(II) to regenerate Fe(III). The initial A^{2-} concentration in non-irradiated SRFA solutions was calculated to be 35.4 μmoles.g^{-1} SRFA based on the measured steady-state Fe(II) concentrations. [3] The calculated value of the standard reduction potential of the A^{-}/A^{2-} couple, based on the measured steady-state concentrations of Fe(II), was +0.59 V (see Garg and co-workers[1] for more details regarding these calculations), which is consistent with the values of standard reduction potential values (0.178-0.734 V) reported for various hydroquinones.[4] However, it should be highlighted that the exact identities of the

organic Fe(II) oxidant and the organic Fe(III) reductant present naturally in SRFA are unclear based on our work but their behavior is consistent with that expected of semiquinone and hydroquinone-like moieties respectively. Nevertheless, it does not preclude the possibility that other functional groups (such as polyphenols) are involved. Note that direct measurement of these groups is not possible due to their low concentration compared to the bulk organic concentration in SRFA.

As described earlier, [1-3] when iron is added to SRFA solution that has been irradiated for 10 minutes (referred to as previously-irradiated SRFA solution) prior to iron addition in the dark, the Fe(II) concentration generated on Fe(III) reduction decreases and the Fe(II) oxidation rate increases compared to that observed in non-irradiated SRFA solution. As shown in Figure 1 and eq. 2, on irradiation of SRFA, superoxide is generated which oxidizes a portion of A^{2-} to A^{-}, thereby resulting in a decrease in the concentration of A^{2-} and increase in the concentration of A^{-}. The transformation of A^{2-} to A^{-}on irradiation results in a decrease in the Fe(III) reduction rate and increase in the Fe(II) oxidation rate when iron is added to previously-irradiated SRFA solution compared to that observed in non-irradiated SRFA solution. The oxidation of A^{2-} by superoxide under our experimental conditions is further supported by redox potential calculations shown in section S3.

$$Q \xrightarrow{h\nu} Q^{*} \xrightarrow{D} Q^{-} \xrightarrow{O_2} HO_2^{\bullet} \qquad (2)$$

where Q represents the redox-active chromophore involved in superoxide generation; D represents the electron donor as described in our earlier work.[5]

When Fe(III) is irradiated in the presence of SRFA (referred as continuously irradiated SRFA solution), Fe(III) reduction mostly occurs via a ligand-to-metal charge transfer (LMCT) pathway with some contribution from intrinsically present hydroquinone-like moieties (A^{2-}) and photochemically generated superoxide. [1-3] Fe(II) oxidation in continuously irradiated

SRFA solution has been observed to occur mostly via formation of superoxide and a short-lived oxidizing entity that has previously been suggested to be peroxyl-type radicals ($RO_2^{\bullet}$) generated via hydroxylation of organic moieties (eq. 3). [1-3]

$$SRFA \xrightarrow[H_2O]{h\nu} "SRFA\text{-}OH^{\bullet}" \xrightarrow[O_2]{} RO_2^{\bullet} \quad (3)$$

Note that here we have summarized the mechanism of Fe redox transformation in acidic SRFA solution as determined in our earlier work;[1-3] refer to these studies for detailed description of the procedure and observations used to determine/support the mechanism presented here.

S2 Additional details on the experimental setup

S2.1: Experimental setup

For investigation of Fe redox transformations in non-irradiated SRFA solutions, appropriate volumes of Fe(III) or Fe(II) stock solutions were added to 30 mL of SRFA solution containing Ca^{2+} in plastic bottles covered with aluminum foil in order to exclude the impact of ambient light. Samples were withdrawn regularly from the reactor and the concentration of Fe(II) was measured using the modified FZ method.[3] For investigation of Fe redox transformations in previously-irradiated SRFA solutions, 3 mL of SRFA solution containing Ca^{2+} was irradiated for 10 min in a 1 cm quartz cuvette followed by addition of appropriate volumes of Fe(II) or Fe(III) stock solutions in the dark. The concentration of Fe(II) remaining or Fe(II) formed at various times after Fe(II) or Fe(III) addition respectively was measured using the modified FZ method.[3] For measurement of Fe redox transformations in continuously irradiated solution, 3 mL of SRFA solution containing Ca^{2+} and Fe(II)/Fe(III) was irradiated in a 1 cm quartz cuvette for 1, 2 5 and 10 minutes and the concentration of

Fe(II) generated or Fe(II) remaining after irradiation was measured using modified FZ method.[3]

S2.2: Fe(II) measurement

For determination of Fe(II) concentration, 60 µL of 50 mM FZ and 5 mM DFB mixture was added to 3 mL of the sample and this solution was continuously circulated through a 1 m path length type II liquid waveguide capillary cell (World Precision Instruments). The absorbance of the solution was measured at 562 nm using an Ocean Optics fiber optic spectrophotometry system with correction for baseline drift by subtracting the absorbance at 690 nm (at which no components of the solution absorb significantly). Calibration of Fe(II) concentrations was performed immediately before undertaking experiments by standard addition of Fe(II) to the buffer solution containing the FZ-DFB mix. A molar absorption coefficient of 27000 $M^{-1}cm^{-1}$ was obtained for $Fe(FZ)_3$ complex which is close to the published value of 27900 $M^{-1}cm^{-1}$.[6] Since a small amount of Fe(III) was reduced by FZ even in the presence of DFB and hence increased absorbance at 562 nm, calibration of Fe(III) was also performed using standard addition of Fe(III) to the buffer solution containing the FZ-DFB mix. The concentration of Fe(II) in the sample was deduced using the equation:

$$[\mathrm{Fe(II)}] = (A_{562} - \varepsilon_{\mathrm{Fe(III)}}[\mathrm{Fe}]_T) / (\varepsilon_{\mathrm{Fe(II)}} - \varepsilon_{\mathrm{Fe(III)}}) \quad (4)$$

where A_{562} represents sample absorbance at 562 nm wavelength, $\varepsilon_{\mathrm{Fe(II)}}$ and $\varepsilon_{\mathrm{Fe(III)}}$ represent molar absorption coefficient of $Fe(FZ)_3$ complex and $Fe(FZ)_3$ formed as a result of reduction of Fe(III) by FZ respectively, and $[\mathrm{Fe}]_T$ represents the total Fe concentration. The detection limit (defined as 3 times the standard deviation of the reagent blank) of the Fe(II) measurement method is ~ 2 nM.

S2.3 Hydrogen peroxide determination

For measurement of H_2O_2 production in irradiated SRFA solutions, 1 mL of sample that was irradiated in a 1 cm quartz cuvette for 1, 2, 5, and 10 min was mixed with 2 mL of 10 mM phosphate buffer (pH = 7.0) followed by addition of 60 µL of AR and HRP mixture and fluorescence was measured using a Cary Eclipse spectrophotometer. Calibration was performed by standard addition of H_2O_2 to 1 mL of non-irradiated SRFA solution mixed with 2 mL of 10 mM phosphate buffer. The detection limit (defined as 3 times the standard deviation of the reagent blank) of the H_2O_2 measurement method is ~ 3 nM.

S2.4: Details of Xe lamp used for SRFA irradiation

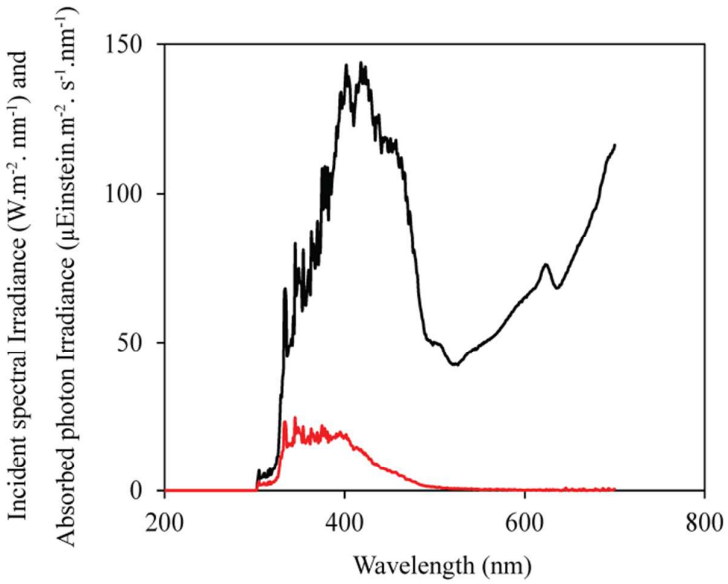

Figure S1: Incident spectral irradiance (black line) and the absorbed photon irradiance (red line) of the Xe lamp used for irradiation of 10 $mg.L^{-1}$ SRFA

S3: Calculation of redox potential for A^{-}/A^{2-} and $HO_2^{\bullet}$ /H_2O_2 couple

To support that the oxidation of A^{2-} by superoxide under experimental conditions investigated here is thermodynamically feasible, the redox potentials for A^{-}/A^{2-} and $HO_2^{\bullet}$ / H_2O_2 couples are calculated. At pH 4, $HO_2^{\bullet}$ is the dominant superoxide species, HA is the dominant semiquinone species and H_2A is the dominant hydroquinone species. Thus, the half- redox reactions and redox potentials are:

$$HO_2^{\bullet} + H^+ + e^- = H_2O_2 \qquad pe_1^0 = 21.24 \qquad (5)$$

$$HA + H^+ + e^- = H_2A \qquad pe_2^0 = 10.17 \qquad (6)$$

$$pe_1 = pe_1^0 - \log\frac{[H_2O_2]}{[HO_2^{\bullet}][H^+]} = pe_1^0 - \log\frac{[H_2O_2]}{\alpha_{HO_2^{\bullet}}[HO_2^{\bullet}]_T[H^+]} \qquad (7)$$

$$pe_2 = pe_2^0 - \log\frac{[H_2A]}{[HA][H^+]} = pe_2^0 - \log\frac{\alpha_{H_2A}[H_2A]_T}{\alpha_{HA}[HA]_T[H^+]} \qquad (8)$$

where $\alpha_{HO_2^{\bullet}}$ represents the fraction of $HO_2^{\bullet}$ concentration, α_{H_2A} represents the fraction of H_2A concentration, and α_{HA} represents the fraction of HA concentration. $[HO_2^{\bullet}]_T$, $[H_2A]_T$, and $[HA]_T$ represent the total concentration of superoxide, hydroquinone, and semiquinone radicals respectively.

At pH 4, $\alpha_{HO_2^{\bullet}} = 0.863$, $\alpha_{H_2A} = 1$, and $\alpha_{HA} = 0.557$. Using the measured total concentration of $HO_2^{\bullet}$ (calculated using the measured H_2O_2 generation rate), H_2O_2, H_2A (calculated based on measured Fe redox transformation in non-irradiated SRFA solution), and HA in our earlier work[1], pe_1 and pe_2 (and corresponding E_H^1 and E_H^2) is calculated using equations S7-S10.

$$pe_1 = 15.27,\ E_H^1 = 0.059 \times pe_1 = 901\ mV, \quad (9)$$

$$pe_2 = 5.12,\ E_H^2 = 0.059 \times pe_2 = 302\ mV. \quad (10)$$

As the redox potential for $HO_2^{\bullet} / H_2O_2$ is higher than that for HA / H_2A, the oxidation of A^{2-} by superoxide under experimental conditions is thermodynamically feasible.

S4: Additional experimental results on Fe redox transformations in previously and continuously irradiated SRFA solution

Table S1: The initial rate of Fe (III) reduction in non-irradiated SRFA solution containing 20 mM Ca^{2+} in the pH range 3-5.

pH	3	4	5
Initial rate of Fe(III) reduction ($nM.min^{-1}$)	4.6 ± 0.4	5.1 ± 2.7	7.6 ± 1.4

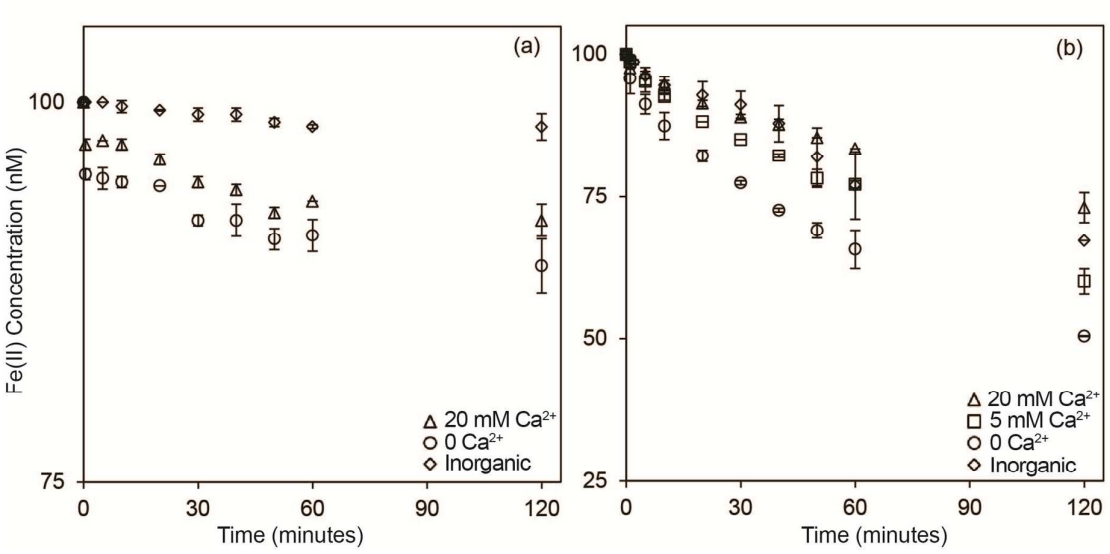

Figure S2: Concentration of Fe(II) remaining as a result of oxidation of 100 nM Fe(II) in 0 $mg.L^{-1}$ SRFA solution (diamonds), 10 $mg.L^{-1}$ SRFA solution (circles), and 10 $mg.L^{-1}$ SRFA solution containing 20 mM Ca^{2+} (triangles) at pH 4 (panel a) and pH 5 (panel b).

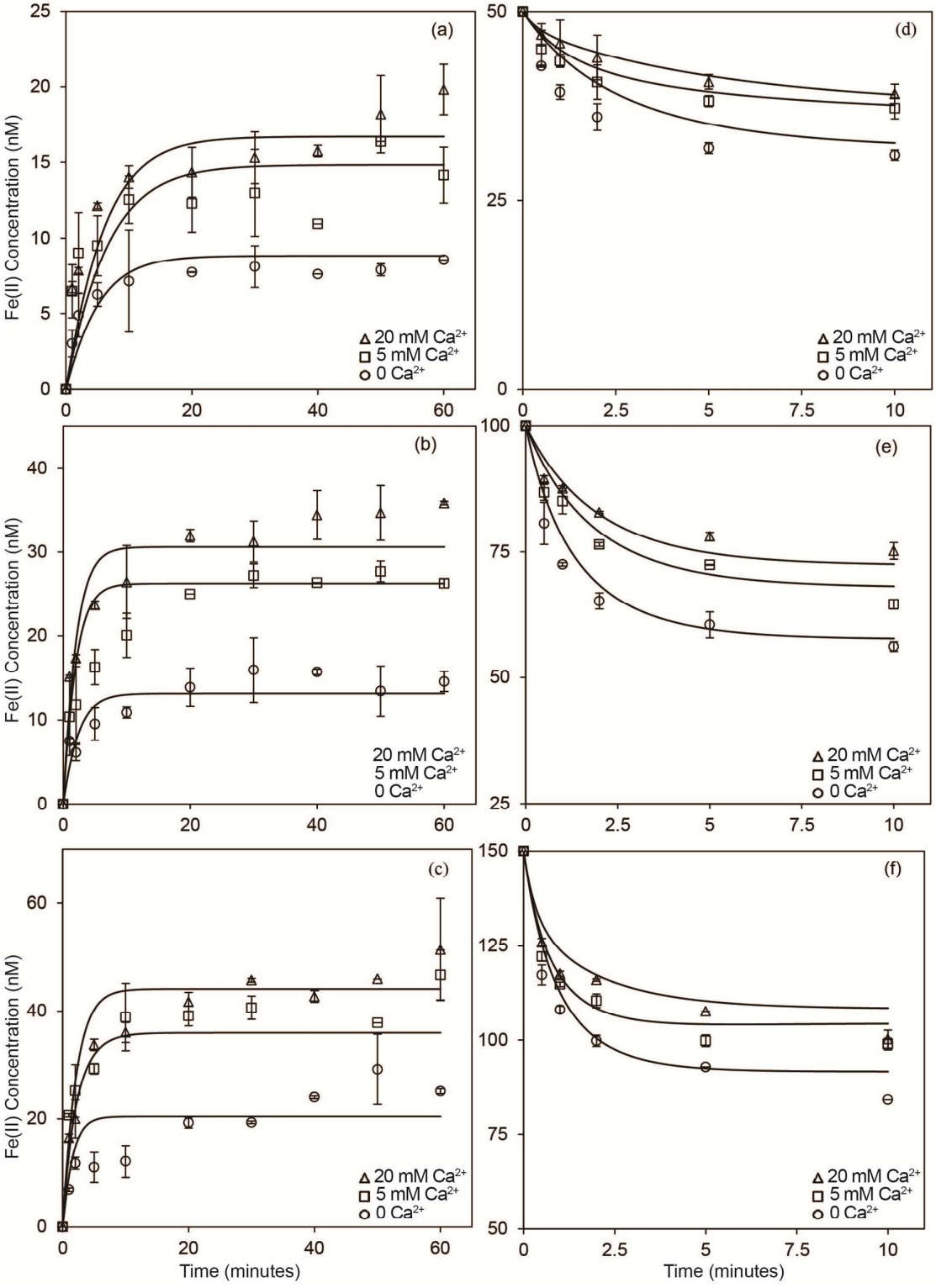

Figure S3: Concentration of Fe(II) generated as a result of reduction of Fe(III) in solution containing 0 (circles), 5 mM (squares), and 20 mM (triangles) Ca^{2+} and 50 nM Fe(III) + 5

mg.L^{-1} SRFA (panel a), 100 nM Fe(III) + 10 mg.L^{-1} SRFA (panel b) and 150 nM Fe(III) + 15 mg.L^{-1} SRFA (panel c) in previously irradiated solution at pH 4. Concentration of Fe(II) remaining as result of oxidation of Fe(II) in solution containing 0 (circles), 5 mM (squares), and 20 mM (triangles) Ca^{2+} and 50 nM Fe(II) + 5 mg.L^{-1} SRFA (panel d), 100 nM Fe(II) + 10 mg.L^{-1} SRFA (panel e) and 150 nM Fe(II) + 15mg.L^{-1} SRFA (panel f) in previously irradiated solution at pH 4. Symbols represent the average of duplicate measurements; lines represent model values.

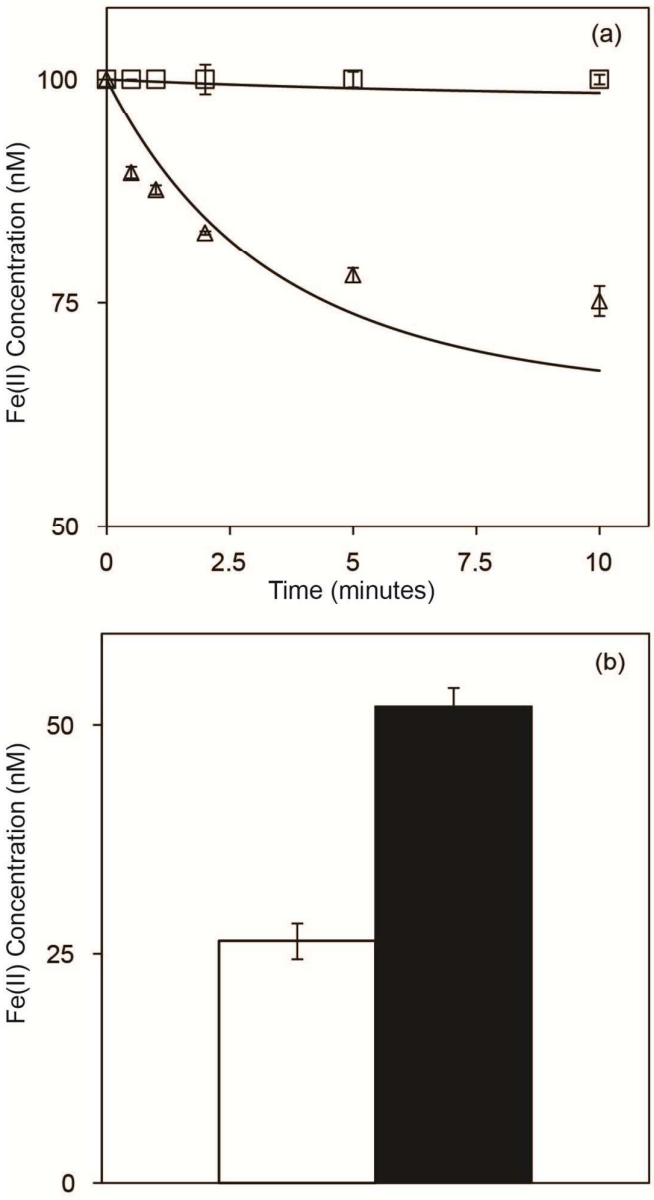

Figure S4: (a) Concentration of Fe(II) remaining as a result of oxidation of 100 nM Fe(II) in previously-irradiated 10 mg.L^{-1} SRFA solution containing 20 mM Ca^{2+} in the presence (squares) and absence (triangles) of 25 kU.L^{-1} SOD at pH 4. Symbols represent the average of duplicate measurements; lines represent model values. (b) Concentration of Fe(II) generated after 10 minutes as a result of reduction of 100 nM Fe(III) in previously-irradiated 10 mg.L^{-1} SRFA solution containing 20 mM Ca^{2+} in the presence (closed) and absence (open) of 25 kU.L^{-1} SOD at pH 4.

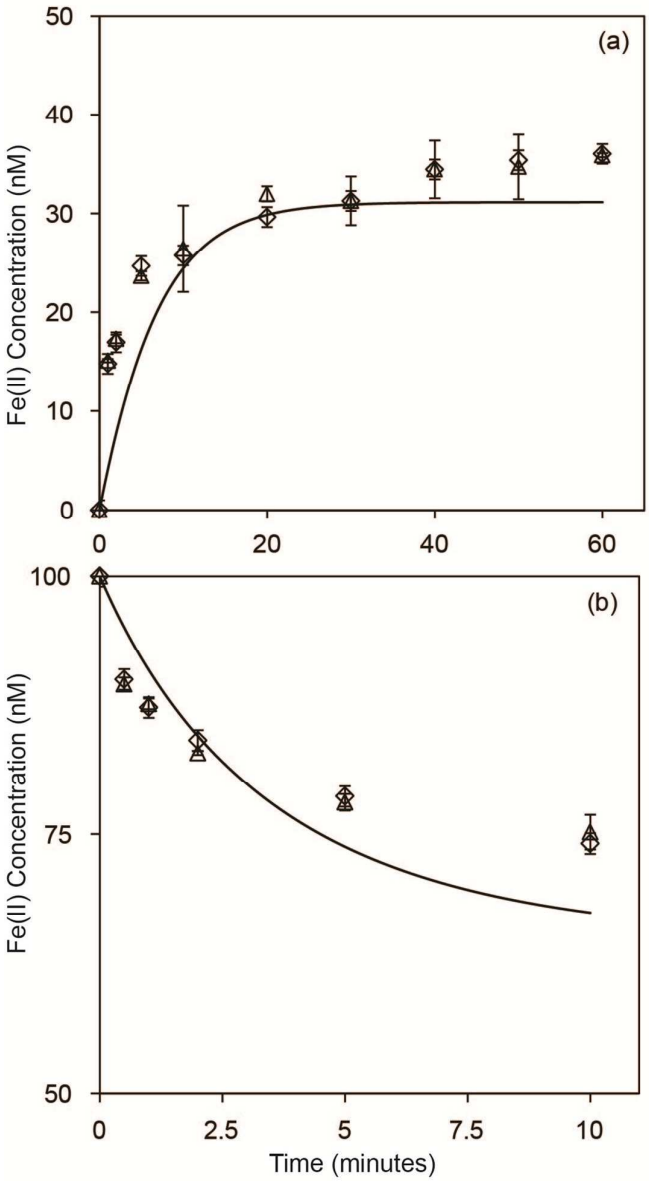

Figure S5: (a) Generation of Fe(II) as a result of reduction of 100 nM Fe(III) in previously-irradiated 10 mg.L^{-1} SRFA solution with addition of 20 mM Ca^{2+} before (diamonds) and after (triangles) irradiation at pH 4. (b) Decrease in Fe(II) concentration as a result of oxidation of 100 nM Fe(II) in previously-irradiated 10 mg.L^{-1} SRFA solution with addition of 20 mM Ca^{2+} before (diamonds) and after (triangles) irradiation at pH 4. Symbols represent the average of duplicate measurements; lines represent model values.

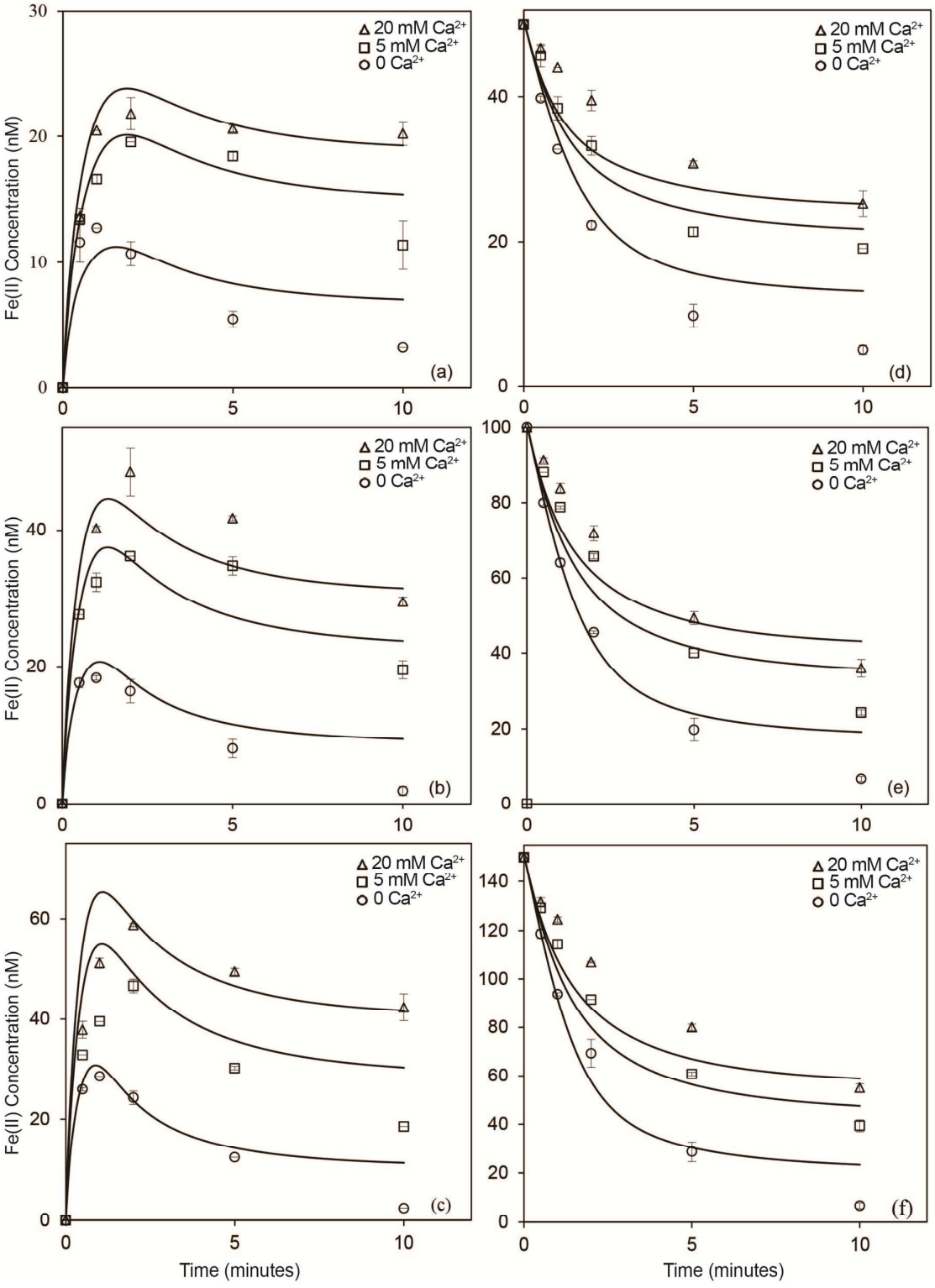

Figure S6: Concentration of Fe(II) generated as a result of reduction of Fe(III) in solution containing 0 (circles), 5 mM (squares), and 20 mM (triangles) Ca^{2+} and 50 nM Fe(III) + 5

mg.L^{-1} SRFA (panel a), 100 nM Fe(III) + 10 mg.L^{-1} SRFA (panel b) and 150 nM Fe(III) + 15 mg.L^{-1} SRFA (panel c) in continuously irradiated solution at pH 4. Concentration of Fe(II) remaining as result of oxidation of Fe(II) in solution containing 0 (circles), 5 mM (squares), and 20 mM (triangles) Ca^{2+} and 50 nM Fe(II) + 5 mg.L^{-1} SRFA (panel d), 100 nM Fe(II) + 10 mg.L^{-1} SRFA (panel e) and 150 nM Fe(II) + 15 mg.L^{-1} SRFA (panel f) in continuously irradiated solution at pH 4. Symbols represent the average of duplicate measurements; lines represent model values.

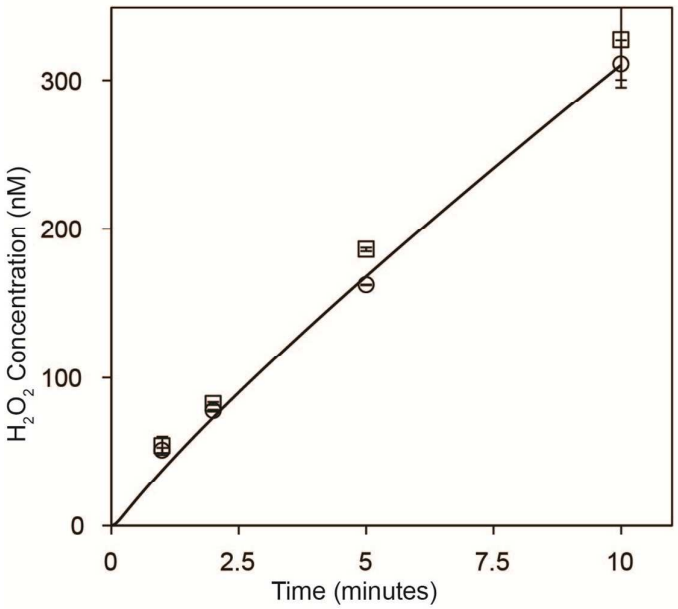

Figure S7: Generation of hydrogen peroxide (H_2O_2) as a result of irradiation of 10 mg.L^{-1} SRFA in the presence (squares) and absence (circles) of 20 mM Ca^{2+} at pH 4. Symbols represent the average of duplicate measurements; lines represent model values.

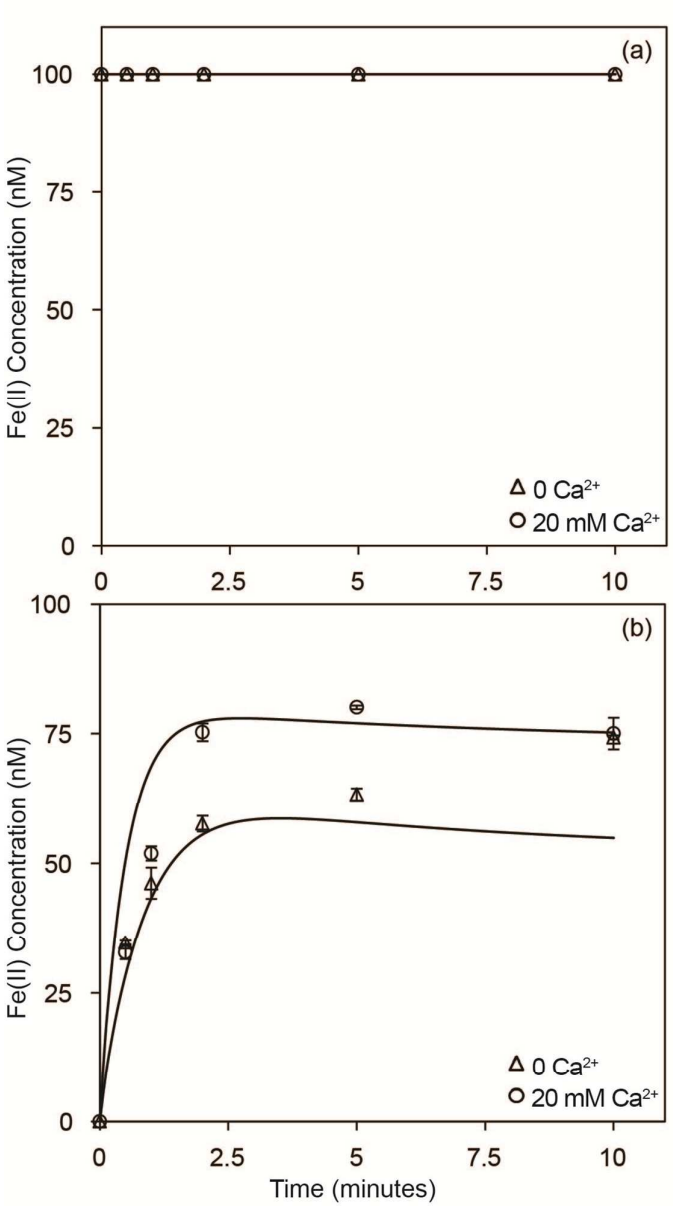

Figure S8: (a) Concentration of Fe(II) remaining as a result of 100 nM Fe(II) oxidation in the presence (circles) and absence (triangles) of 20 mM of Ca^{2+} in the presence of 25 $kU.L^{-1}$ SOD in continuously- irradiated SRFA solution at pH 3. (b) Generation of Fe(II) as a result of 100 nM Fe(III) reduction in the presence (circles) and absence (triangles) of 20 mM of Ca^{2+} in the presence of 25 $kU.L^{-1}$ SOD in continuously- irradiated SRFA solution at pH 3. Symbols represent the average of duplicate measurements; lines represent model values.

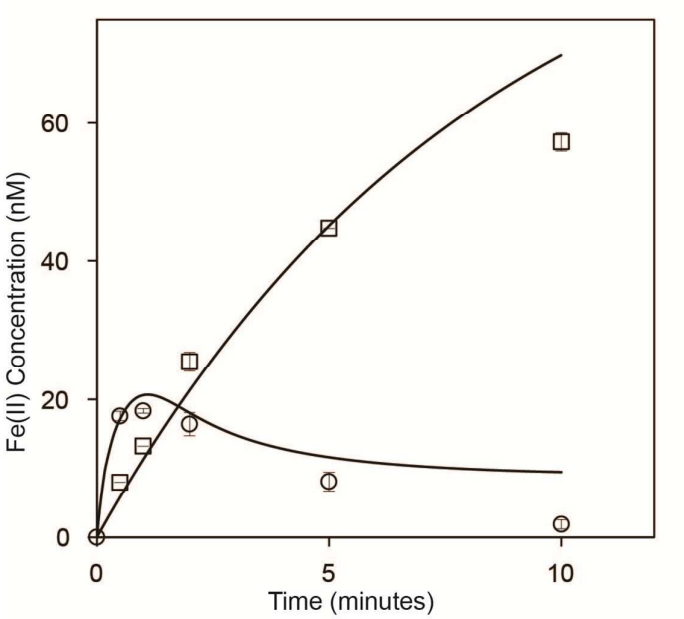

Figure S9: Concentration of Fe(II) generated as a result of reduction of 100 nM Fe(III) in continuously irradiated solution in the presence (circles) and absence (squares) of 10 $mg.L^{-1}$ SRFA. Symbols represent the average of duplicate measurements; lines represent model values.

Note that even though higher Fe(II) concentration is measured in the absence of SRFA especially during the later stages due to very slow Fe(II) oxidation rate in these solution; however as indicated in the Figure S9, the initial Fe(III) reduction rate is higher in the presence of SRFA since Fe(II) oxidation becomes increasingly important during later stages.

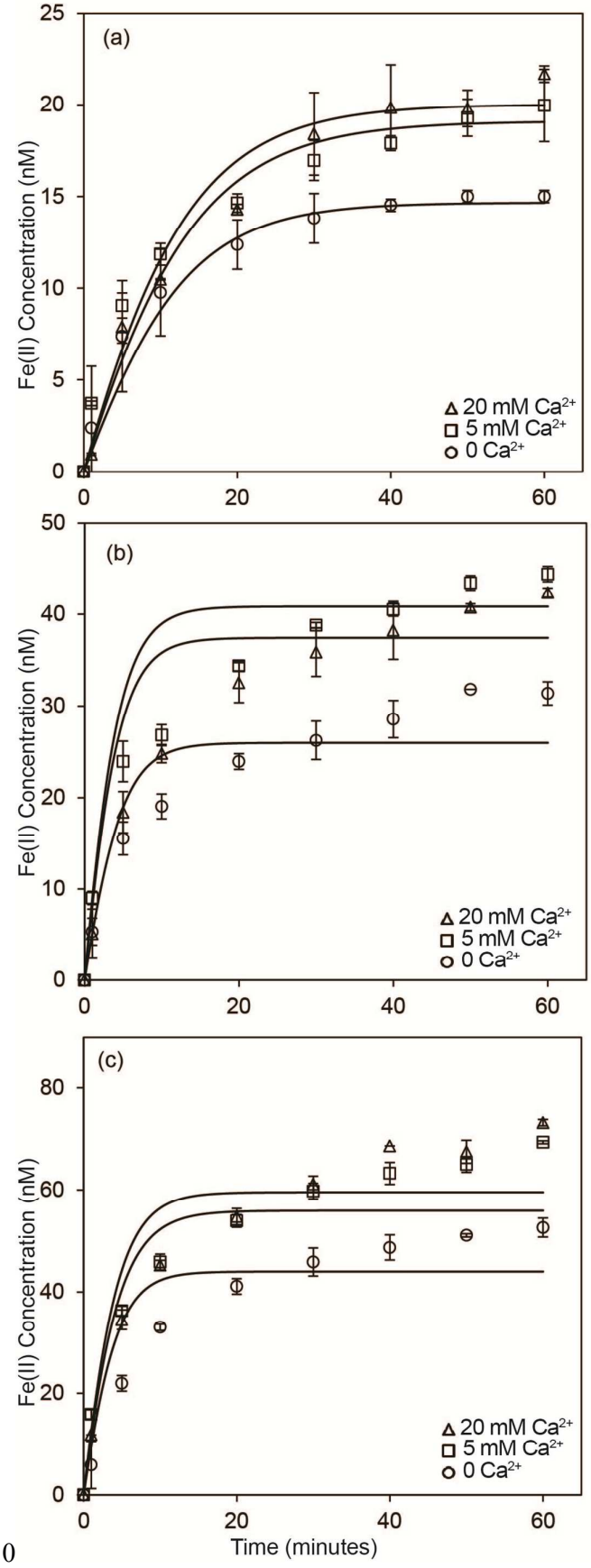
(a)
Fe(II) Concentration (nM)
20 mM Ca2+
5 mM Ca2+
0 Ca2+
(b)
Fe(II) Concentration (nM)
20 mM Ca2+
5 mM Ca2+
0 Ca2+
(c)
Fe(II) Concentration (nM)
20 mM Ca2+
5 mM Ca2+
0 Ca2+
Time (minutes)

Figure S10: Generation of Fe(II) as a result of reduction of Fe(III) in solution containing 0 (circles), 5 mM (squares), and 20 mM (triangles) Ca^{2+} and 50 nM Fe(III) + 5 $mg.L^{-1}$ SRFA (panel a), 100 nM Fe(III) + 10 $mg.L^{-1}$ SRFA (panel b) and 150 nM Fe(III) + 15$mg.L^{-1}$ SRFA (panel c) in non-irradiated solution at pH 4. Symbols represent the average of duplicate measurements; lines represent model values.

S5: Detailed description of the kinetic model

As shown in figures 2-4 in the main manuscript, the kinetic model shown in Table 1 provides an excellent description of experimental results under various conditions including varying pH under both irradiated and non-irradiated conditions. A brief summary of the key reactions as well as justification of rate constants used is provided below.

S5.1 Instantaneous establishment of steady-state singlet oxygen concentration

Upon irradiation, photo-excited SRFA reacts rapidly with dioxygen in triplet state to form singlet oxygen (reaction 1; Table 1), which undergoes relaxation on interaction with the solvent to form triplet state oxygen (reaction 2). The rate constants for reactions 1 and 2 used here are same as reported earlier.[7]

S5.2 Superoxide formation during irradiation

Formation of superoxide occurs as a result of reduction of triplet state dioxygen by O_2-reducing radical Q^- (reaction 4; Table 1), which is formed on reduction of quinone moieties (Q) on irradiation (reaction 3; Table 1). The rate constant for reactions 3 (Table 1) was determined based on best-fit to our experimental results and the rate constant for reaction 4 (Table 1) used here is same as that reported in our earlier study.[1] The concentration of Q was assumed to be same as the electron accepting capacity of SRFA;[8] however note that the concentration of Q is not well constrained by our experimental data with a similar fit obtained using varying concentrations with suitable adjustment of the rate constant for the reaction 3.

S5.3 Uncatalyzed disproportionation of superoxide

As described in reaction 5 (Table 1), H_2O_2 is formed as a result of uncatalyzed disproportionation of superoxide with the rate constant for this reaction varying with pH as reported earlier by Bielski et al.[9]

S5.4 Oxidative superoxide sink

Superoxide also decays due to interaction with organic moieties generated on irradiation of SRFA (see reactions 6-8 in Table 1). The rate constants for the superoxide decay is pH dependent due to the different reactivity of O_2^- and $HO_2^\bullet$. The rate constant for these reaction used here are same as that reported in our previous study.[1]

S5.5 Transformation of hydroquinone and semiquinone-like moieties on irradiation

The transformation of hydroquinone (A^{2-}) to semiquinone-like radicals (A^-) occur on interaction with photochemically generated superoxide. Superoxide plays a role in both oxidizing A^{2-} to A^- (reaction 9; Table 1), as well as reducing A^- to reform A^{2-} (reaction 10; Table 1). The rate constants for reactions 9 and 10 were reported in our previous study[1] with reaction 10 independent of pH and reaction 9 varying with pH to predict the varying concentration of A^{2-} and A^- formed after irradiation at different pH. Rate constant for reaction 10 is slightly different to that reported in our earlier work[1] and determined based on best-fit to our experimental results. Semiquinone-like radicals (A^-) is further oxidized by singlet oxygen to form quinone (A) and superoxide (reaction 11; Table 1). The rate constant for this reaction is used as determined in our earlier work.[1]

S5.6 Peroxyl radical generation

Generation of the short-lived Fe(II) oxidant on irradiation, peroxyl radicals ($RO_2^\bullet$) is described by reaction 12 (Table 1), and its bimolecular decay and unimolecular decay are described by reaction 13 and 14 (Table 1) respectively. The rate constants for reactions 12-14 were reported in our previous study,[1] and are varied slightly here based on best-fit to our experimental results.

S5.7 LMCT mediated Fe(III) reduction

Reactions 15 and 16 represent the LMCT-mediated reduction of strongly and weakly complexed Fe(III) occurring under irradiated conditions. The rate constants for these reactions were obtained via best-fit to our experimental results (Figure 4). The rate constant for LMCT-mediated reduction of weakly-complexed Fe(III) (reaction 16) is approximately 2-times higher than that for strongly-complexed Fe(III) (reaction 15).

S5.8 Superoxide mediated Fe(III) reduction

As discussed in the main manuscript, superoxide-mediated Fe(III) reduction (SMIR) also contributes (10-20%) to Fe(II) generation under continuously irradiated condition. The rate constant for SMIR (reaction 17; Table 1) was used as reported earlier[10] for SRFA complexed Fe(III). The rate constant for SMIR on weakly-complexed Fe(III) (reaction 18; Table 1) is not well-constrained by the kinetic model, with same model output for rate constant in the range 2×10^5 - 4×10^5 $M^{-1}s^{-1}$.

S5.9 Peroxyl radical mediated Fe(II) oxidation

Fe(II) oxidation in continuously-irradiated SRFA solution occur via its interaction with peroxyl-like radicals (reaction 19; Table 1). The rate constant for Fe(II) oxidation by peroxyl radicals was assumed to be pH-independent and was same as that described in our earlier work. [1] The rate constant for weakly complexed Fe(II) oxidation by peroxyl radicals (reaction 20; Table 1) is not well-constrained by the kinetic model, with same model output for rate constant in the range 5×10^6 - 1×10^7 $M^{-1}s^{-1}$.

S5.10 Superoxide mediated Fe(II) oxidation

Fe(II) oxidation by superoxide (reaction 21; Table 1) was assumed to be pH dependent, with rate constants varying due to changes in superoxide speciation and are same as that reported in our earlier study. [1] The rate constant for weakly complexed Fe(II) oxidation by superoxide

(reaction 22; Table 1) is not well-constrained by the kinetic model, with same model output for rate constant in the range 0.5 k_{21} - k_{21} (where k_{21} represents the rate constant for superoxide-mediated oxidation of strongly-complexed Fe(II)).

S5.11 Hydroquinone mediated Fe reduction

Interaction of Fe(III) with hydroquinone-like moieties are presented in reactions 23 and 24 (Table 1) with the rate constants determined based on best-fit to our experimental results. Rate constant for Fe(III)L reduction by A^{2-} (reaction 24) is considered to be independent of pH due to the invariant speciation of hydroquinone and Fe(III) in the pH range investigated. The rate constants for reduction of weakly-complexed Fe(III) (reaction 24; Table 1) is approximately 2 times higher than that for strongly-complexed Fe(III) (reaction 23) which is consistent with the LMCT-mediated reduction rate of strongly and weakly complexed Fe(III).

S5.12 Fe(II) oxidation by semiquione-like radicals

Interaction of Fe(II) with semiquinone-like moieties are presented in reactions 25 and 26 (Table 1) with the rate constants determined based on best-fit to our experimental results. The rate constant for Fe(II) oxidation by A^- is pH dependent due to the variation in A^- species (HA / A^-, pK_a ~4) with pH as described in the following equation:

$$k_{26} = \alpha_0 k_{HA} + \alpha_1 k_{A^-} \quad (11)$$

where k_{HA} and k_{A^-} represent rate constants for Fe(II) oxidation by HA and A^- respectively and α_0 and α_1 represent molar fraction of HA and A^-, i.e. $\alpha_0 = \frac{[H^+]}{[H^+] + K_{HA}}$, and $\alpha_1 = 1 - \alpha_0$ with $K_{HA} = 10^{-4}$. k_{HA} and k_{A^-} are 2.4 × 10^4 $M^{-1}s^{-1}$ and 1.4 × 10^5 $M^{-1}s^{-1}$ respectively.

The Fe(II) oxidation rate constant of weakly-complexed Fe(II) formed in the presence of Ca^{2+} (reaction 26) was determined based on best-fit to our experimental results and was approximately half of that measured for Fe(II) complex formed in the absence of Ca^{2+}.

S5.13 Fe(II) oxidation by dioxygen

The rate constants for Fe(II) oxidation by dioxygen at pH 3 and 4 are not included in the model, as the experimental results showed that Fe(II) oxidation by dioxygen is very slow at pH ≤ 4. However, at pH 5, Fe(II) oxidation by dioxygen becomes important with Fe(II) half-life of approximately 2 h. The rate constants for reaction 27 and 28 are determined on the basis of the best fit to the measured Fe(II) oxygenation rate in non-irradiated SRFA solution (Figure S2b). The ratio of k_{27} / k_{28} is 2, suggesting 20 mM Ca decreased Fe(II) oxygenation rate by 50%, very close to the effect of 20 mM Ca^{2+} on Fe(II) oxidation rate by other oxidants, such as $HO_2^{\bullet}$ and semiquinone-like moieties.

S6: Calculation of diurnal cycle of Fe cycling rate

To calculate the Fe cycling rate over the whole diurnal cycle, we assumed 12h: 12 h light: dark period. Furthermore, the light intensity was assumed to vary sinusoidally, with the peak light intensity observed at 12 pm. To reflect the effect of light intensity on Fe transformation in irradiated condition, the rate constants for reactions involving photo-generation of organic moieties and ROS (superoxide and singlet oxygen) and LMCT mediated Fe(III) reduction were assumed to vary linearly with the light intensity. For example, the light intensity at 8 am is 50% of the maximum light intensity at midday, and the corresponding rate constant for Fe(III) reduction by LMCT (reaction 15; Table 1) was adjusted to 3.75×10^{-3} s^{-1}, half of the reported value. Similarly, the rate constants for reactions 1, 3, 6, 12, and 16 (Table 1) were also adjusted to 50% of the reported rate constants in Table 1 for the calculation of TOF at 8 am. The Fe cycling rate in dark was determined based on its interaction with hydroquinone and semiquinone-like moieties.

References

1. Garg, S.; Jiang, C.; Waite, T. D., Mechanistic insights into iron redox transformations in the presence of natural organic matter: Impact of pH and light. *Geochim. Cosmochim. Acta* **2015,** *165*, 14-34.
2. Garg, S.; Jiang, C.; Miller, C. J.; Rose, A. L.; Waite, T. D., Iron redox transformations in continuously photolyzed acidic solutions containing natural organic matter: Kinetic and mechanistic insights. *Environ. Sci. Technol.* **2013,** *47*, 9190-9197.
3. Garg, S.; Ito, H.; Rose, A. L.; Waite, T. D., Mechanism and kinetics of dark iron redox transformations in previously photolyzed acidic natural organic matter solutions. *Environ. Sci. Technol.* **2013,** *47*, (4), 1861-1869.
4. Roginsky, V.; Barsukova, T., Kinetics of oxidation of hydroquinones by molecular oxygen. Effect of superoxide dismutase. *J. Chem. Soc., Perkin Trans. 2* **2000**, 1575-1582.
5. Garg, S.; Rose, A. L.; Waite, T. D., Photochemical production of superoxide and hydrogen peroxide from natural organic matter. *Geochim. Cosmochim. Acta* **2011,** *75*, 4310-4320.
6. Stookey, L. L., Ferrozine---a new spectrophotometric reagent for iron. *Anal. Chem.* **1970,** *42*, 779-781.
7. Paul, A.; Hackbarth, S.; Vogt, R. D.; Röder, B.; Burnison, B. K.; Steinberg, C. E. W., Photogeneration of singlet oxygen by humic substances: comparison of humic substances of aquatic and terrestrial origin. *Photochem. Photobiol. Sci.* **2004,** *3*, 273-280.
8. Aeschbacher, M.; Sander, M.; Schwarzenbach, R. P., Novel electrochemical approach to assess the redox properties of humic substances. *Environ. Sci. Technol.* **2010,** *44*, 87-93.
9. Bielski, B.; Cabelli, D.; Arudi, R.; Ross, A., Reactivity of HO_2/O_2^- radicals in aqueous solution. *J. Phys. Chem. Ref. Data* **1985,** *14*, 1041-1100.
10. Garg, S.; Rose, A. L.; Waite, T. D., Pathways contributing to the formation and decay of ferrous iron in sunlit natural waters. In *Aquatic Redox Chemistry*, ACS symposium series: 2011; Vol. 1071, pp 153-176.